Massachusetts Institute of Technology

MASSACHUSETTS INSTITUTE OF TECHNOLOGY
Final Scientific/Technical Report

PowerChip: Advanced Technologies for Integrated Power Electronics
Agile Delivery of Electric Power Technology (ADEPT)
DE-FOA-0000288

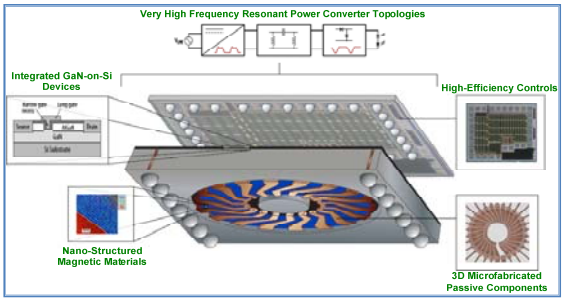

Award:	DE-AR0000123
Lead Recipient:	Massachusetts Institute of Technology
Project Title:	PowerChip: Advanced Technologies for Integrated Power Electronics
Program Director:	Prof. David J. Perreault
Principal Investigator:	Prof. David J. Perreault
Contract Administrator:	Mr. Gary DesGroseilliers
Date of Report:	March 31, 2014
Reporting Period:	September 1, 2010 – December 31, 2013

Public Executive Summary

To realize advances in power conversion technology, the research project investigated three areas:) new power semiconductor devices; 2) new magnetic materials and component designs; and 3) new circuit architectures and topologies to realize higher degrees of miniaturization, integration and performance. The application focus was on power converters for driving LED loads, encompassing ac-to-dc and dc-to-dc conversion from moderate voltage levels (to above 100 V) to low voltages (e.g., tens of Volts) at low to moderate operating power levels (e.g., tens of Watts). Semiconductor device research focused on the performance, reliability and improved design of devices based on Gallium Nitride (GaN). Magnetics research focused on both development of new magnetic materials suitable to higher operating frequencies and on microfabrication of magnetic components. Systems research focused on leveraging these advances to attain higher operating frequencies, miniaturization and performance as compared to the present state of the art. We summarize each of these thrusts below.

DEVICES. Many new fabrication technologies and device structures have been made over the course of this program to improve the state-of-the-art of GaN. These advances were made to address a wide variety of issues in GaN devices including threshold voltage control, field plates for increased breakdown voltage, multi-finger layout for wide periphery devices, and device packaging.

Threshold voltage control was an important aspect of this project. Enhancement mode (positive V_t) devices are highly desirable for power electronics as they can simplify circuit design and improve system reliability. Even when depletion mode-devices were used, uniform threshold voltage control was still critical, since the V_t needed to be shifted to a level suitable for the high speed gate driver. At the beginning of this project, a single gate recess of the AlGaN barrier was used to push threshold voltage positive. This technology suffered from high off-state leakage, which was remedied by adding a tri-gate structure under the gate. These e-mode recessed, tri-gate devices coupled with SiO_2 gate dielectric were able to achieve an off-state ID below 1 μA/mm for drain voltages up to 600 V. However, precise control of the barrier etch depth of the gate recess was challenging using a timed etch. Timed gate recess etches resulted in non-uniformity of etched barrier thickness and thus variation of threshold voltage across large samples. Furthermore, the plasma etching used to recess (necessitated by the lack of effective wet etch chemistries for AlGaN) could introduce damage, increase the density of defect states and degrade the channel mobility. A special epitaxial structure with an etch-stop layer was employed to solve these problems. With these wafers, a highly selective dry etch was used to remove the barrier down to an AlN etch-stop layer; then a subsequent wet etch removed the plasma damaged AlN resulting in reproducible e-mode HEMTs with low interface state density. This technology received the IEEE George Smith Award for best paper published in IEEE Electron Device Letters during 2012.

Field plate and passivation technology had to also be optimized to meet the switching and blocking voltage demands of the power converter circuit. Surface passivation was needed to reduce the occurrence of surface traps that deplete the channel and cause the dynamic on-resistance phenomena. However, after passivation and reduction of the surface state depletion, the electric field in the channel is less uniformly spread, which significantly reduces the breakdown voltage of the devices. A field plate is needed to smooth electric field and prevent low voltage breakdown of the device. In this project, we experimentally optimized the passivation dielectric (plasma enhanced chemical vapor deposition silicon nitride) thickness under source connected field plate to achieve the optimal breakdown voltage performance.

For use in the power converter circuit developed for this project, the GaN devices had to sustain current levels in excess of 1 A with minimal on-resistance, so large periphery multi-finger transistors were required. A robust multi-finger transistor process was made targeting the issues of reducing individual transistor finger resistance, developing a reliable interlayer dielectric via etch, and implementing an interconnect metallization scheme to support the required current levels. With this multi-finger transistor technology, we were able to design and fabricate a variety of device peripheries in layouts suitable for packaging. The initial packaging technique was wire bonding the GaN HEMT to pads of a discrete package. However, this was quickly abandoned in favor of a flip-chip solder ball bumping technology, where the device is placed directly on the circuit board, eliminating the separate package and reducing parasitic inductance by removing the wire bonds.

A combination of these technologies allowed us to fabricate GaN transistors with W_g= 40 mm and W_g= 80 mm and integrate them into a program dc-dc power converter stage operating at high frequency. At lower power levels (below 20 W), the W_g=40 mm devices yielded high efficiency in the test converter. At higher power levels, the device performance was limited by heat dissipation. Improved thermal management is needed to extend the high performance obtained below 20 W to higher power levels.

DEVICE RELIABILITY. This aspect of the project has pursued a detailed investigation of electrical reliability and trapping of High-Voltage GaN FETs for power switching applications. Our research has revealed that in GaN MIS-HEMTs for operation >600 V, current collapse is the main concern. We have observed extreme trapping leading to total current collapse after OFF-state stress at high voltage. This trapping process is completely recoverable, is accelerated by increasing drain-to-source stress voltage and does not exhibit temperature dependence. The mean time to trapping exhibits a typical Zener-like electric field dependence. This phenomenon is attributed to high-field tunneling-induced electron trapping ("Zener trapping") inside the AlGaN barrier or the GaN channel layers. The trapping takes place in a narrow region right under the edge of the outermost field plate in the drain portion of the device. This finding gives urgency to defect or impurity control during epitaxial-growth and the design of appropriate field plate structures for the reliable high-voltage operation of GaN MIS-HEMTs.

We have investigated current collapse in prototype AlGaN/GaN MIS-HEMTs fabricated on a 6-inch Si wafer by our industrial collaborator, Texas Instruments. In the OFF-state, when VDS exceeds approximately 200 V, we observe trapping that is so severe that it leads to total current collapse and the device effectively behaves as an "open" when subsequently biased in the ON state. This behavior is fully recoverable and repeatable.

To gain greater insight into this phenomenon, we studied the voltage dependence of the dynamics of trapping. We performed constant OFF-state stress tests at different voltages and measured the time evolution of normalized linear drain current I_{Dlin} (roughly equal to inverse of ON resistance, a key figure of merit in power switching devices). I_{Dlin} degradation greatly speeds up as VDS stress voltage increases from 140 V to 180 V at room temperature. In this experiment, we define a characteristic trapping time τ at 50% degradation of I_{Dlin}. We plot τ vs. $1/E_{PEAK}$ where E_{PEAK} is the peak value of electric field inside the AlGaN barrier layer under the edge of the outermost field plate estimated from field simulations by Silvaco. This is the characteristic Zener tunneling law. The excellent linearity that is obtained strongly suggests a valence-band-to-trap tunneling process. We call this "Zener trapping." A trap energy level of around 1 eV above the valence band edge is estimated from this study.

We also explored the role of temperature on this trapping behavior by performing identical OFF-state step-stress experiments at different temperatures from 25 to 200°C. The trapping characteristics are found to be insensitive to temperature and the evolution of the four terminal currents over the entire temperature range confirming again that they are not the main source of electron trapping. The temperature insensitivity of the phenomenon again suggests that trapping takes place through a tunneling process.

Additional studies of the role of the geometrical design of the device, the impact of UV light of different wavelengths on the detrapping dynamics and electric field simulations has allowed us to synthesize a simple picture for this phenomenon. Once the OFF state voltage exceeds the voltage required to deplete underneath the outermost field plate of the device, any further increases in voltage sharply increase the electric field at the surface of the device right underneath the edge of the field plate. This field can get so intense that electrons can tunnel directly from the valence band to traps in the bandgap of the AlGaN barrier or GaN channel. This is what we term as "Zener tunneling." When the device is brought to the ON state, the trapped electrons create a barrier to current flow through the channel effectively turning off the device.

We further postulate that these traps are associated with the yellow photoluminescence widely observed in GaN and AlGaN. This is believed to arise from C dopants. C is also a common dopant in the buffer structure of GaN high-voltage FETs and has a location inside the energy bandgap which is consistent with many observations made in our study.

The detailed understanding that has been derived about the observed total current collapse mechanism suggests that proper defect control during epitaxial growth and appropriate design of the field plate structures are essential to mitigate this effect.

MAGNETICS

The magnetics aspect of the research encompassed design optimization and performance prediction, microfabrication of winding structures for coreless and cored designs, development of novel magnetic materials and magnetic core designs, and full magnetic component construction and component testing, including in full converter systems. The work was coordinated across four institutions – Dartmouth, Georgia Institute of Technology, MIT, and University of Pennsylvania. We describe work broken down approximately by institution, but note that there was substantial coordination and collaboration across the different institutions to accomplish the results achieved.

Dartmouth – *W*ork on magnetics by the Dartmouth group focused on utilizing sputter-deposited Co-Zr-O nanocomposite soft magnetic cores to make high-power-density, high-efficiency inductors. Two technologies were developed. The first technology was a "racetrack" inductor with an elongated spiral winding sandwiched between two layers of low-loss Co-Zr-O nanocomposite soft magnetic material. For these inductors, advanced loss modeling and optimization techniques were developed, as well as a new fabrication technique to produce controlled-slope sidewalls for the "magnetic vias" connecting top and bottom magnetic layers. Fabricated components achieved inductance values of 1.2 µH and peak quality factors of 15.1 at 8.3 MHz. They were successfully demonstrated in the LED driver circuit, which achieved 89% efficiency at 5 MHz with the inductors operating at 1 W output per mm^2 of substrate area.

A new concept for higher performance inductors was also proven in this work. A constraint in utilizing many advanced magnetic materials such as Co-Zr-O is its uniaxial anisotropy – they only work well for flux travel in one direction. This prevents effective utilization in the otherwise ideal toroidal geometry in which flux travels in a circular path, changing direction continuously around the path. It was demonstrated that applying a radial field during deposition could produce a material with local anisotropy oriented exactly as needed for high performance. Inductors fabricated with these materials achieved a Q value of over 50 throughout the 10 to 50 MHz range, and were successfully demonstrated in the baseline LED driver, which achieved higher than 96% efficiency with these components.

Georgia Institute of Technology – The GIT group focused on fabrication issues associated with reducing the size/footprint and increasing the integration capability of power inductors fabricated on semiconductor or other substrates. In particular, a new microfabrication scheme was developed to realize three-dimensional windings for solenoid and toroid inductors. These inductors were fabricated both with air-cores in collaboration with the MIT group, and with magnetic-cores separately developed commercially, and at GIT, Dartmouth and U Penn. These inductors were successfully demonstrated in the baseline led driver as described below.

A key microfabrication advance was the exploitation of thick metal encapsulation of polymer pillars to form vertical via interconnections for three-dimensional windings. The radial conductors of the toroidal inductor were formed by conventional plating-through-mold techniques, while the vertical windings (up to 1000 µm in height) were formed by polymer cores with metal plated on their external surfaces. This encapsulated polymer approach not only significantly reduced the required fabrication time, but also exploited the relative ease of fabricating high-aspect-ratio SU-8 pillars as opposed to high-aspect-ratio SU-8 trenches. To form the top radial conductors, non-photopatternable SU-8 was introduced as a thick sacrificial layer.

Based on this microfabrication advance, inductors with multiple permutations of the following geometries and cores were fabricated: solenoid and toroid, on-glass and embedded-silicon, and air core and magnetic core. Inductors showed typical inductances of 60-800 nH and typical small-signal Q-factors of 8-45, depending on the geometry and magnetic material.

For baseline LED driver testing (undertaken at MIT), inductors with microfabricated windings and air cores, as well as various magnetic cores, were developed including: 1) CoNiFe highly laminated cores from GT with microfabricated and hand-wound windings; 2) CoZrO cores from Dartmouth with microfabricated and hand-wound windings; 3) commercial iron powder cores with silicon-embedded windings; and 4) Fe_3O_4 nanogranular powder toroids from U Penn.

1. CoNiFe highly laminated cores (fabricated as part of a GIT-led parallel ADEPT program) were introduced where the core geometry is compatible with solenoid inductor windings. These CoNiFe inductors were tested in the baseline LED driver. Microfabricated-winding and hand-wound inductors demonstrated a power converter efficiency of 93% at 100-V continuous fan-cooled operation.

2. CoZrO cores from Dartmouth were integrated with 25-turn microfabricated and hand-wound inductors from GIT, and tested in the baseline LED driver. These devices showed an efficiency of 92.6% at 50-V pulsed operation and 94% at 100-V continuous operation, respectively.

3. Commercial iron-powder cores were integrated with silicon-embedded microfabricated windings from GIT to form a silicon-embedded inductor. This device was tested in the baseline power converter and showed 92% efficiency at 50-V pulsed uncooled operation.

4. Fe_3O_4 nanogranular powder toroids from U Penn were integrated with 25-turn hand-wound toroidal inductors and showed 94% efficiency at 100-V continuous operation.

Massachusetts Institute of Technology – The MIT group focused on the analysis and optimized design of microfabricated toroidal air-core inductors. Central to this effort was an advanced approach to modeling the energy stored and the power dissipated in the inductors. Inductors embedded in insulating substrates and in silicon were both considered. For both choices of

substrate, the energy stored in the internal toroidal core, in the external space surrounding the inductor, and in the winding separating those two regions were all modeled. For inductors embedded in silicon, magnetically-driven and electrically-driven losses in the silicon were modeled in addition to the magnetically-driven losses in the winding present for both choices of substrate. The winding loss model was specifically derived to account for the increased loss arising from the typically large separation between adjacent winding turns in a microfabricated inductor. An equivalent-circuit model suitable for circuit simulation was used to summarize the modeling results.

The equivalent-circuit inductor model was combined with a circuit model of the baseline LED driver to analyze the performance of the driver for a given inductor design. This system analysis was then combined with Monte Carlo synthesis to analyze driver performance over a wide range of inductor designs and transistor size scaling. Pareto-optimal filtering was used to manage the competing design metrics of driver efficiency, inductor size, and minimum microfabrication feature size. Microfabrication feature size was considered as a proxy for inductor microfabrication yield. The resulting optimizing design code was then exercised to identify a Pareto optimal design frontier for the inductors from which several designs were selected for microfabrication and testing. Collaboration with GIT provided reasonable fabrication constraints to limit the inductor design space.

Several toroidal air-core inductors were microfabricated by GIT, and tested both individually and in the baseline LED driver. Inductor performance was very well predicted by the models, typically to within several percent, over a wide frequency range; the modeling accuracy of energy storage and power dissipation was generally much better than that of traditional modeling approaches. In terms of inductor performance, it was observed that microfabricated toroidal air-core inductors with a diameter ranging from 8 to 10 mm, and a height of 1 mm, could support a baseline LED driver that meets the program objectives.

University of Pennsylvania – The U Penn magnetic-materials group worked to develop several innovative routes to prepare nanocomposite materials having high permeability but low loss when driven at high frequencies (e.g., 3-30 MHz). In traditional polycrystalline magnetic materials, large or irregular crystal grain size and strong magnetic and electrical coupling between these grains has resulted in unacceptable high “hysteresis losses” or electrical eddy current losses. One way to overcome these limitations might be to create an ensemble of magnetic grains nearly identical to each other in size and shape and space them apart by a desired amount using a thin insulator. The goal is to space the grains an ideal amount to keep them from communicating too much with each other magnetically or electrically, while maintaining a high density of magnetic material to realize the desired permeability. In this ARPA-E project the U Penn group explored a chemical route to realize this idealized system.

The U Penn group worked to synthesize nanometer-sized crystals (nanocrystals) of magnetic materials that could be used as magnetic inks/moldable powders that would allow the

integration of the magnetic materials into fabricated micro-inductors. The group succeeded in developing methods to synthesize, purify and stabilize new families of size- and shape-controlled ferrites, metals and metal alloy nanocrystals. Each resulting sample was small enough to behave as single domain magnetic structures to allow high permeability (μ/μ_0 =10 to 30) and was encapsulated with a monolayer of cross linkable organic insulator to provide better mechanical cohesion and to suppress electrical losses due to eddy currents induced in the magnetic core. These nanocomposite materials displayed low loss (tan $\delta < 0.025$) for drive frequencies up to 5 MHz. Procedures were developed to scale the production of the solution of possible nanocomposites from just a few hundred mg in the discovery phase of the project to production of up to batches of 10 grams needed to build a series of prototype devices. These solutions of possible nanocomposites were integrated into toroidal micro-inductors and tested in converter test platforms, enabling operation at 5-MHz with efficiencies exceeding 93% at power loads of 40 Watts. This combination of synthesis, integration/fabrication and testing drew from skills across the spectrum of the ARPA-E PowerChip team and has provided a motivation to pursue integration of chemically produced magnetic nanocomposites as a means of introducing magnetic function in the "back-end" of microelectronics fabrication.

Magnetics Summary – In summary, the magnetics team comprising all four institutions collectively demonstrated that microfabricated inductors are feasible components for integrated power electronics. In particular, several inductors were demonstrated in the baseline LED driver, and shown to support driver performance that met the program requirements. Moreover, in contrast to the magnetic components typically found in commercial the power converters, the microfabricated inductors demonstrated in this project were not the largest components in the converter, nor were they responsible for a significant majority of the converter losses.

CIRCUITS AND SYSTEMS. This aspect of the research, carried out principally at MIT, focused on developing circuit architectures, topologies and designs that could leverage the advances in devices and components to achieve higher performance (and especially greater miniaturization) while meeting the needs of practical systems (e.g., high efficiency, low electromagnetic interference, high power factor for ac-interfaced systems, etc.). Achieving increased operating frequency while maintaining high efficiency was a key research focus, as higher frequencies are needed to realize the degree of miniaturization desired for future systems. While not required by the program, attention was also paid to realizing ac-interface systems that could operate at high power factor without the need for electrolytic capacitors (which often pose temperature and lifetime limits) and to achieving miniaturized power converters that could function efficiently across wide voltage ranges. Lastly, a focus of this work was quantitative testing and evaluation of program and commercial semiconductor devices and magnetics, and use of the results to advance knowledge and for modeling and optimization of systems.

A first result of the circuits and systems investigation is a merged-two-stage circuit architecture and associated topology that is useful for designs working in the high-frequency (HF) regime (3-

30 MHz, or approximately 5-50 x that of typical designs in this space). The design is suitable for either wide-range dc input voltage or ac line input, though it is more suited to the former function than the latter. This two-stage approach is based on a soft-charged switched-capacitor pre-regulator / transformation stage and a high-frequency magnetic regulator stage. Soft charging of the switched capacitor circuit, zero voltage switching of the high-frequency regulator circuit, and time-based indirect current control are used to maintain high efficiency, high frequency and power density, and (where relevant) high power factor. The proposed architecture has been applied to an LED driver circuit, with two implementations demonstrated: 1) a wide input voltage range dc-dc converter and 2) a line-interfaced ac-dc converter. The prototype dc-dc converter achieves 88-96% efficiency at 30 W power across 25-200 V input voltage range. The ac-dc converter achieves 88% efficiency with 0.93 power factor at 8.4 W average power.

A second result of the circuits and systems investigation is a new power conversion architecture for single-phase ac grid interface. The proposed architecture is suitable for realizing miniaturized ac-dc converters operating at high frequencies (HF, above 3 MHz) and high power factor, without the need for electrolytic capacitors. It comprises a line-frequency rectifier, a stack of capacitors, a set of regulating converters, and a power combining converter (or set of power combining converters). The regulating converters have inputs connected to capacitors on the capacitor stack, and provide regulated outputs while also achieving high power factor, with twice-line-frequency energy buffered on the capacitor stack. The power combining converter combines power from the individual regulated outputs to a single output, and may also provide isolation.

While the architecture described above can be utilized with a variety of circuit topologies, it is especially suited for systems operating at HF, and we developed an implementation that enables efficient operation in this range. The proposed approach is demonstrated for an LED driver operating from 120 Vac, and supplying a 35 V, 30 W output. The prototype converter operates at a (variable) switching frequency of 5–10 MHz and an efficiency of > 93%. The converter achieves a displacement power density of 130 W/in^3, while providing a 0.89 power factor, without the use of electrolytic capacitors. The extremely high performance provided by this prototype has motivated development of this architecture for a broad range of applications.

Acknowledgements

The authors gratefully acknowledge the financial support and guidance for this work provided by ARPA-E under the Agile Delivery of Electric Power Technology (ADEPT) program (DE-FOA-0000288) through grant DE-AR0000123. As part of this, the guidance and oversight by ARPA-E staff and related support staff – including Dr. Mark Hartney, Dr. Timothy Heidel, Dr. Mark Johnson and Dr. Scott Litzelman – are greatly appreciated. The authors would also like to acknowledge material support (including test devices) provided by Texas Instruments, and advice and input provided by FINsix corporation.

The Principal Investigator was David J. Perreault at MIT. Members of the research team at MIT included Mohammad Araghchini, Jesus A. del Alamo, Gary DesGroseilliers, Jingying Hu, Donghyun Jin, Sameer Joglekar, Alex Jurkov, Jeffrey H. Lang, Seungbum Lim, Bin Lu, David Otten, Tomas Palacios, Daniel Piedra, John Ranson, and Min Sun. Researchers at Dartmouth College included Daniel Harburg, Christopher G. Levey, Jizheng Qiu, Charles R. Sullivan, Rui Tian, and Di Yao. Researchers at Georgia Institute of Technology included Mark Allen, Florian Herrault, Chang-Hyeon Ji, Jungkwun Kim, and Xuehong Yu. Researchers at the University of Pennsylvania were Jun Chen, Vicky Doan-Nguyen, Christopher B. Murray, and Hongseok Yun.

Table of Contents

Table of Figures/Tables

Accomplishments and Objectives

This award allowed the PowerChip team to demonstrate a number of key objectives. The focus of the project was on developing device, passive component and circuit/system technology for high-frequency miniaturized power electronic converters.

A number of tasks and milestones were laid out in Attachment 3, the Technical Milestones and Deliverables, at the beginning of the project. The actual performance against the stated milestones is summarized here:

Table 1. Key Milestones and Deliverables.

Major Tasks	Key Milestones and Deliverables
Program Element 1: Nitride device development and system integration **1.1**: Increase of breakdown voltage **1.2**: Reduction of on resistance **1.3**: Threshold voltage control **1.4**: Integration **1.5**: Reliability assessment	**Q1**: Development of device simulation, mask design & geometry optimization, initial fabrication of GaN HEMTs. Test structures for reliability assessment designed. **Completed 11/30/2010** The mask set for the nitride devices was designed and produced to include test structures and multi-finger devices. The final mask design included devices with 40 mm and 80 mm gate periphery (optimized to reduce on-resistance) as well as material characterization structures and devices for reliability testing. **Q2**: First batch of multifinger devices with breakdown voltage of 200 V fabricated and tested. **Completed 2/28/2011** The initial batch of depletion mode multi-finger devices with a range of gate widths up to W_g= 39.6 mm were successfully fabricated and tested. Breakdown voltage tests of early devices show V_{bk} ~ 320 V for multi-finger devices. Electrical stress set-up up to 1000 V completed. **Completed 2/28/2012** Automatic electrical stress and characterization environment which can handle voltage up to 3000 V has been established. This includes Agilent B1505A power semiconductor analyzer and Cascade Tesla probe station. **Q3**: E-mode devices with on-resistance below 4 Ω.mm fabricated and tested. **Completed 5/31/2011** Enhancement mode devices were fabricated and tested. At this point in the project, a sub-micron gate recess etch in the barrier was used to achieve positive threshold voltages. However, the

Major Tasks	Key Milestones and Deliverables
	on-resistance of these e-mode devices was ~10 Ω.mm as the L_{ds} spacing was increased to meet required breakdown voltage levels. This higher resistance did not impact the final circuit performance significantly. Reliability assessment of 200 V FETs under OFF (200 V) and ON (2 V) conditions completed. **Completed 5/31/2011** Large electron trapping has been observed that drastically degrades device performance in 200 V FETs. Relevant degradation mechanism has been proposed. **Q4**: Second batch of multifinger devices with breakdown voltage of 600 V fabricated and tested. Polarization engineering demonstrated for threshold voltage control and E-mode operation demonstrated. **Completed 8/31/2011** The second batch multi-finger devices were fabricated and tested. Although single finger devices showed breakdown voltage up to 643 V, ultimately 200 V multi-finger devices were used in circuit demonstration, as these devices could have a smaller LDS and thus a smaller on-resistance. Gate recess etching showed more promise as a threshold voltage control method than polarization engineering. Thus, efforts were focused on improving the manufacturability of the gate recess process rather than the polarization engineering. **Q5**: Complete analytical studies of design space for device fabrication. **Completed 11/30/2011** Based on results from initial tests and system simulation, it appeared valuable to have devices of 80 mm gate periphery and "half-sized" devices of 40 mm gate periphery. In this way, we could trade-off on-resistance for capacitance and see the effect on the overall circuit efficiency. **Q7**: Gate leakage at V_{DS}=600 V reduced below 10 μA/mm through gate dielectric technology. **Completed 12/31/2011** Using the tri-gate enhancement-mode approach, devices demonstrated gate leakage levels from 10^{-5} μA/mm to 10^{-2} μA/mm throughout a 600V sweep using ALD SiO_2 gate dielectric.

Major Tasks	Key Milestones and Deliverables
	Q10: Threshold voltage control with hydrogen passivation demonstrated. Fourth batch of multifinger devices with breakdown voltage of 600 V, threshold voltage > 2 V and leakage current below 10 mA fabricated and tested. **Completed 3/01/2013** Threshold voltage control through hydrogen passivation was unstable and was thus not pursued further since the alternative e-mode gate recess methods were more promising. Although single finger devices showed breakdown voltage up to 643 V, ultimately 200 V multi-finger devices were used in circuit demonstration, as these devices could have a smaller LDS and thus a smaller on-resistance. These devices showed leakage current below 10 mA (in the range of 0.1 mA – 1 mA). Dynamic on-resistance modeled and key parameters affecting it identified. Third batch of multifinger devices with breakdown voltage of 600 V and threshold voltage > 2 V fabricated and tested. **Completed 10/01/2012** The key parameter affecting the dynamic on-resistance is the presence and quality of surface passivation. 200 V multi-finger devices were used in circuit demonstration (with V_t shifted to ~ -3V) to minimize on-resistance and optimize circuit efficiency. Development of process technology and mask set for single chip integration. **Completed 11/30/2012** The group moved away from single chip integration to focus on an implementation using discrete devices that highlighted our advanced packaging method (flip-chip bonding as opposed to wire-bonding). **Q12**: Fifth batch of multifinger devices optimized for integration with Si control electronics and passive components. Device characterization completed. **Completed 8/31/2013** The fabrication and characterization of the final batch of multi-finger devices optimized for integration with Si control electronics and passive components was completed. These devices featured a tri-gate structure, sub-micron barrier recess, source-connected field plate, silicon nitride passivation, and flip-chip solder ball bumping. Reliability assessment of 600 V FETs under OFF (600 V) and ON (2 V) conditions completed. **Completed 6/01/2013**

Major Tasks	Key Milestones and Deliverables
	Excessive electron trapping triggered at high voltage has been identified as dominant degradation phenomenon. A trapping mechanism has been suggested. **Q13:** Structural analysis of 600 V devices completed; failure mechanisms identified. **Completed N/A** Electron trapping has been identified as dominant failure mechanism. This is not expected to induce any structural degradation in the devices. Detailed structural analysis on 600 V devices is not necessary. **Q14:** Primary failure drivers and scaling laws identified. **Completed 12/31/2013** Total current collapse phenomenon triggered by electric field has been identified to be a primary failure driver for high voltage GaN power transistors. We attribute this to high-field tunneling-induced electron trapping ("Zener trapping") inside the AlGaN barrier or the GaN channel layers. Trap energy levels around 1 eV above valence band is estimated and carbon dopant is suspected as the responsible trapping site. Lifetime model completed. **Completed 12/31/2013** Physical laws and dominant time constants and activation energies for trapping and detrapping of electrons in traps responsible for Zener trapping have been determined.
Program Element 2: Magnetic materials and components **2.1**: Microfabricated three-dimensional windings and magnetics **2.2**: Nanogranular magnetic materials and components **2.3**: New magnetic materials and synthesis methods **2.4**: Magnetics modeling, design, and optimization	**Q1**: Initial models for toroidal air-core and nanogranular inductors magnetics completed. The air-core models improve on previous models by incorporating displacement current effects that arise with the component embedded in a Si substrate; the nanogranular inductor models address the newly proposed configuration. **Completed 11/30/2010** Two significant improvements to the traditional models for toroidal air core inductors were incorporated. The first improvement involved an energy-based method for determining the magnetic fields inside the toroidal core. This method specifically accounted for the gaps between the winding turns, and explained the current crowding observed at the edges of the turns at the gaps. From the fields, an equivalent surface current in the winding was determined, and this surface current was extended into the winding according to the physics of magnetic diffusion. This in turn led to an improved determination of winding losses. The second improvement involved introducing a

Major Tasks	Key Milestones and Deliverables
	model for the displacement currents in a silicon substrate into which an embedded toroidal inductor was fabricated. These currents are driven by the spatial and temporal variation of electric potential from winding turn to winding turn. The current models in turn permitted the determination of conduction losses in the silicon and an increase in the parasitic capacitance along the inductor. The initial nanogranular inductor model addressed racetrack inductors in both surface and embedded configurations, and included first order models of inductance, core loss, and winding loss based on AC and DC resistance. Synthesis equipment for new magnetic materials configured. **Completed 12/13/2010** Synthesis equipment with 3 L size reactor for large scale reaction was successfully installed. **Q2**: Initial designs for nanogranular and air-core inductors completed. **Completed 2/28/2011** An automated computer code was created to design inductors. The code permitted both fixed and variable design parameters, and synthesized the variable design parameters randomly in a Monte-Carlo sense. The performance of each designed inductor was then determined using the previously developed models, and inductor performance was filtered in a Pareto-Optimal sense to identify a performance frontier along which the best inductors could be found. It is important to note that the computer-based design code included a model of the power converter so that the performance of each inductor, and the converter using that inductor, could be judged. Initial inductor designs were based on estimated fabrication constraints and material properties, and were intended to test the models, the fabrication processes and the subsequent test procedures. They were not specifically intended to meet the specifications required by the program. They were approximately 6 mm to 24 mm in diameter, and 0.5 mm tall. Automated computer code was also developed for nanogranular inductors, using particle-swarm optimization to find a Pareto frontier of options for power density and efficiency. Initial nanogranular inductor designs were for a 15 MHz operating frequency in a 25 W converter, using a 458 nH embedded racetrack inductor.

Major Tasks	Key Milestones and Deliverables
	First generation air-core inductor fabrication initiated. (First generation air-core inductors are for use in model verification, for developing key fabrication steps, and for identifying fabrication challenges.) **Completed 12/31/2010** For the first generation air-core inductor model, three different inductors were investigated: 1) silicon-embedded; 2) through-silicon; and 3) on-glass. The key microfabrication steps including deep silicon etching, proximity lithography and 3D copper electroplating, along with validating each inductor model developed at MIT. 20 μm thick nanogranular magnetic materials deposited. **Completed 11/01/2010** A sample of Co-Zr-O film was deposited successfully with no adhesion problems observed; measurements are reported below, under third task in Q3. Testing systems for new magnetic materials configured. **Completed 3/28/2011** With Agilent 4395A and magnetic materials test fixture 16454, the relative permeability of magnetic nanoparticles could be measured from 100 kHz to 500 MHz. **Q3**: Initial designs for nanogranular core inductors completed. Nanogranular material process steps mapped out. **Completed 6/15/2011** Initial nanogranular inductor designs, as described above in first task of Q2, were for a 15 MHz operating frequency in a 25 W converter, using a 458 nH embedded racetrack inductor. This was predicted to have 0.4 W power loss and 5.7 pF capacitance. A fabrication process for these embedded inductors was planned out using 12 fabrication steps. Designs for nanogranular core targeted three methods: 1) doctor blading deposition; 2) drop casting deposition; and 3) pressed nanoparticle disk through high pressure pressing after ligand exchange. Fabrication of first-generation air-core inductors completed. Inductor winding is continuous and has no turn-to-turn or turn-to-substrate short circuits. **Completed 5/31/2011** On-glass inductor and silicon-embedded inductor were

Major Tasks	Key Milestones and Deliverables
	successfully fabricated. Both inductor windings were continuous and did not observed turn-to-turn or turn-to-substrate short circuits. 20 µm thick nanogranular magnetic materials tested and plan developed to address any performance shortcomings relative to targets of hard-axis permeability greater than 50 and hard-axis coercivity less than 5 Oe with 0.5 T peak excitation. **Completed 3/31/2011** Permeability was measured as 120, and, at a drive level of 0.5 T peak, coercivity was measured as 0.9 Oe, meeting the target with a large margin. The coercivity was measured as a function of drive level showing even smaller coercivity at lower drive levels. **Q4**: Demonstration that the developed models are able to predict performance of the air-core inductors, including inductance, loss and resonance frequency. **Completed 8/31/2011** Two methods were used to determine the accuracy of the models, with a focus on losses; most models, including those developed here, are quite accurate in terms of determining inductance. The first method was a comparison with finite-element analysis. The second method was a comparison with experimental data. A library of 2D geometrically-linear finite-element analyses was created to determine the losses in windings having different ratios of width to thickness and skin depth to thickness. The ratios were chosen to match those anticipated for the project. The losses determined from the simulations were then compared to the losses determined with the models developed here, and to the losses determined with a simple skin depth model. Generally, the losses determined with the models developed here matched those from the library to with 3% or less, while the error in the losses determined with the simple skin depth model ranged from 5% to 35%. An early 100-nH microfabricated inductor was testing in a converter, and its current and voltage waveforms were measured. These waveforms were used to extract an equivalent inductance and resistance (loss). These parameters were compared to hose predicted by the models developed here. The inductances matched to with 2-3% while the resistance showed a considerable difference. It was determined that the wire bonds between the inductor and the power converter contributed significant resistance requiring further analysis.

Major Tasks	Key Milestones and Deliverables
	On-glass inductor and silicon-embedded inductor were characterized in terms of inductance, resistance, and quality factor. The on-glass inductor was approximately 650 µm tall with an outer diameter of 6 mm and 25 winding turns. The inductance, dc resistance and quality factor showed approximately 90 nH and 250 mΩ, and 15 at 10 MHz respectively. The silicon-embedded inductor was approximately 400 µm tall with an outer diameter of 6 mm and 25 winding turns. The inductance, dc resistance and quality factor showed approximately 60 nH and 300 mΩ, and 6 at 10 MHz respectively. 20 µm nanogranular films exhibit good magnetic performance as measured on B-H loop tracer. Specifically, hard-axis permeability should be greater than 50, and hard-axis coercivity should be less than 5 Oe with 0.5 T peak excitation. **Completed 3/31/2011** The initial tests reported above in third task of Q3 already met this objective so no additional work was needed to meet this milestone. Design of radial magnet array finalized. **Completed 6/22/2011** A magnetic array was optimized by finite-element analysis to achieve a radial field in the region of the toroidal core. The radial component of the field was at least 10 times as strong as the axial component throughout the target region. The field strength was at least 100 mT, much stronger than the target of 40 mT. Later work developed a second-generation fixture with similar performance for smaller samples, less than 5.6 mm OD. **Q5**:Second-generation air-core designs developed that meet the requirements of one or more topologies specified under program element 3. Key design factors to be met include inductance, loss and self-resonant frequency. (In addition to meeting early design requirements, the second generation is to produce devices that can be used with hybrid packaging, and to address any processing difficulties encountered in the fabrication of first-generation designs.) **Completed 11/30/2011** The focus of this task was on inductors microfabricated on an insulating substrate. The models were improved to incorporate fabrication limitations observed during the fabrication of the first-generation inductors. Inductors were designed for a power

Major Tasks	Key Milestones and Deliverables
	converter handling 25 W; the converter frequency was estimated to be in the range of 5-8 MHz. The inductors had a 650 um height, and ranged in radius from 8-15 mm. The winding turn-turn gap was 50 um, and the winding turn thickness was either 50 or 100 um. Total converter efficiency near 91% was predicted. An alternative fabrication approach was proposed for the air-core inductors. While we demonstrated that the first generation inductor fabrication approaches are feasible, and the fabricated devices exhibited good results, the process was time consuming due to the bottom-up plating of the high-aspect-ratio vias. As a result, we propose a different approach that relies on metalized polymer bone vertical vias. This process has dramatically reduced the fabrication process time. The very thick via copper plating process (~650 um) was replaced by a 20 to 40 um thick electroplating step of the vias. This was possible because the vias have a SU8 polymer bone (or core) structure, and plating is initiated from the sidewall. In summary, we replaced a bottom up plating process by sidewall plating. For silicon-embedded inductor, we have been developing an interconnection scheme compatible with the fabrication process of the si-embedded inductors for ultimate compactness and high level of integration. 30-50 μm nanogranular film deposition demonstrated. **Completed 6/01/2012** The first samples deposited in this thickness range had 40 μm of radial anisotropy Co-Zr-O material on thin toroidal Si substrates. Because of problems with thermal mismatch with the thin substrates, these exhibited low yield (37%). Later samples deposited on almunina substrates had high yield (typically >80%). Radial magnet array constructed. **Completed 7/15/2011** Fixtures were fabricated for 8-mm inner diameter (min), 16-mm outer diameter (max) toroidal substrates. The fixtures included two permanent magnets, steel pole pieces, and a copper substrate support that also serves as a heat sink. Correlation of metal nanocrystal structure and loss validated in new magnetic materials. **Completed 1/30/2012** Spherical and cubic nanocrystals such as nickel, iron oxide, zinc ferrite, nickel ferrite, and nickel zinc ferrite were tested to validate the correlation between the nanocrystal structure and loss with the

Major Tasks	Key Milestones and Deliverables
	PPMS (Physical Property Measurement System) up to 10 kHz and spheres expressed less loss than cubes. **Q6**: Second-generation air-core inductor fabrication initiated. **Completed 2/01/2012** The fabrication for both on-glass and silicon-embedded inductors were initiated. Toroidal samples of nanogranular films deposited and tested. **Completed 12/01/2011** Toroidal samples were deposited, first on polyimide substrates. To verify radial anisotropy, small square samples were cut from the toroid, and measured in a B-H loop tracer. They showed the desired radial anisotropy, whereas samples cut from a control sample deposited without a radial field were nearly isotropic, with large hysteresis loops. This shows that the desired orientation was achieved and that it had the desired result of reducing hysteresis loss. Complex permeability was also measured and showed flat real relative permeability near 60 and Q over 100 below 50 MHz. Ferrite-based new magnetic materials deposited and tested. Magnetic moment and AC susceptibility characterized to 1MHz. AC electrical resistance of film characterized to 100MHz. **Completed 5/31/2012** AC susceptibility of 6 nm nickel zinc ferrite was tested from 1 MHz to 1 GHz with the permeameter at Dartmouth. Due to small size of nickel zinc ferrite nanoparticles, susceptibility was quite low (between 1 and 2). Electrical resistance of nickel ferrite film was characterized from 10 kHz to 10 MHz and the result clarified the high resistance of nanoparticle film. (~400 k Ohm at 10 MHz). **Q7**:Second-generation air-core inductor fabrication completed. Inductors are functional, meeting design specifications (inductance, loss, voltage breakdown), and suitable for use in a converter with hybrid packaging. **Completed 5/31/2012** The fabrications of second-generation air-core inductors were completed. 50 turn on-glass inductor showed an inductance of approximately 200 nH in the frequency range of 0.1-100 MHz, dc resistance of 0.8 Ω, and quality factor of 8 at 10 MHz while 25 turn inductor showed 80 nH, 200 mΩ, and 18 at 10 MHz respectively. The inductors were tested to full voltage and they

Major Tasks	Key Milestones and Deliverables
	did not breakdown. In subsequent testing throughout the course of this project, electrical breakdown was never observed to be a problem and it ceased to be a focus during testing. **Q8**: Third-generation air-core designs developed that meet the refined (optimized design) requirements from program element 3. (In addition to meeting refined design requirements, the third generation is targeted to produce devices that address integration with other components.) **Completed 8/31/2012** 3rd generation air-core inductors were developed. The inductors consist of 70 turns, with an outer diameter of 8 mm and inner diameter of 4 mm. The inductors are approximately 1 mm in height. The manner in which the inductors were microfabricated was improved. In particular, the vias were plated around patterned insulating pillars which permitted much taller inductors. Correspondingly, the models of inductor loss were changed. In addition, revised microfabrication limitations, most notably minimum feature sizes, were incorporated in the computer-based design code. Finally, for silicon-embedded inductors, models of magnetically-driven losses in the silicon substrate were included. Further small improvements to most models were incorporated in the computer-based design code. With the improved models, inductors for full-power converter operation and were designed. The projected efficiency ranged from 92-94% depending on the thickness of the inductor. However, it was observed that the efficiency was strongly dependent on inductor temperature, and inductor temperature was hard to predict for the lighting application. As a result, a high temperature of 125 C was used during the design process, and this led to large air core inductors having radii near 10 mm. First generation nanogranular-core magnetics tested. Tests include dc resistance and complex impedance as a function of frequency, and will be compared to design values established in Q3. **Completed 9/07/2012** Based on problems with the embedded racetrack inductor fabrication process, a surface racetrack process was developed in parallel. The surface racetrack fabrication process was found to be superior, but measured performance was not yet satisfactory. Inductance was lower than the design value, quality factor was low (peaking around 7), and inductance rolled off at frequencies above 10 MHz. The causes of these problems were traced to fabrication issues, addressed immediately below in third task of Q8.

Major Tasks	Key Milestones and Deliverables
	Second-generation nanogranular-core designs developed. These designs should either improve at least one performance metric by at least 20% or address processing difficulties encountered in the fabrication of first-generation designs. **Completed 9/28/2012** Problems with the initial fabrication process included inadequate insulation between the top corners of the winding and the top core layer, and poor control over the shape of sloped SU-8 insulation. To solve these problems, we developed process and design improvements including thicker SU-8 insulation and a UV-LED/prism exposure system for achieving nearly ideal 45-degree angled exposure of SU-8. Detailed design optimizations were also re-run based on the updated magnetics and circuit models. Third-generation air-core magnetics fabrication initiated. **Completed 5/31/2012** The fabrication of the third-generation air-core inductor was initiated. Plans for process integration of new magnetic materials finalized. **Completed 8/31/2012** We established routes to process colloidal magnetic nanoparticles into thick films and free standing disks that could be integrated into hand wound toroidal inductors. As of 01/07/2014 we are pushing to demonstrate drop casting of magnetic backfills into prefabricated MEMS inductors but this work is expected to take until 01/30/2014 to complete. A drop-in approach for the process integration of new magnetic materials was also investigated, and successfully tested with other materials. **Q10**: 30-50 μm nanogranular films exhibit good magnetic performance as measured on B-H loop tracer. Specifically, hard-axis permeability should be greater than 50, and hard-axis coercivity should be less than 5 Oe with 0.5 T peak excitation. **Completed 3/29/2013** Several samples with thicknesses in this range were deposited with good performance found in a wide range of tests, including B-H loops, small-signal complex permeability, and performance in inductors. Specifically for this milestone, a 40 μm thickn sample was measured in a B-H loop tracer, with the data corrected for demagnetizing factor. Demagnetizing factor was extracted

Major Tasks	Key Milestones and Deliverables
	from a set of measurements and also found from a finite-element simulation in order to ensure that this correction was applied properly for an unusual shape sample. (The sample was a set of two adjacent rectangles, patterned with the mask used for racetrack inductors.) Coercivity at 0.5 T peak excitation was 2.6 Oe based on the best estimate of demagnetizing factor, or 3.5 Oe based on the worst case value of demagnetizing factor. Fabrication of second-generation nanogranular-material-based inductors completed. **Completed 10/13/2012** A 3" wafer of inductors was completed and partially diced for further testing in first task of Q11. Scale production of new ferrite based magnetic materials to 10-gram quantities. **Completed 9/20/2012** 6 nm nickel zinc ferrite nanoparticles could be synthesized more than 5 g from a single batch. By combining 2 or more batches of nanocrystal reaction, more than 10 gram scale production was achieved. **Q11**: Testing of second-generation nanogranular-material-based inductors completed. Tests include dc resistance and complex impedance as a function of frequency, and will be compared to design values established in Q8. **Completed 5/31/2013** DC resistance and complex impedance measurements matched design and modeled values very closely. Peak quality factors were about 18, slightly higher than predicted. Scale production of new metallic magnetic materials to 10 gram quantities. **Completed 12/31/2013** By combining two or more reaction batches, the production of nickel nanoparticles in different sizes was scaled up to 10 gram quantities. **Q12:** New magnetic materials produced in 10-gram quantities tested. FeCo alloy NCs produced at 10g scale for integration and prototyping. Size target below 20nm with less than 8% dispersion. Loss at 10MHz pushed to match sputtered Co-Zr-O benchmark. **Completed N/A**

Major Tasks	Key Milestones and Deliverables
	Due to oxidation issues/stability, the synthesis of nanocrystals we chose to focus all efforts on metal oxide nanocrystals. Iron oxide nanoparticles from 8.7 nm to 17.8 nm in size could be produced at 10 g scale their relative permeability values were characterized. **Q14**: Materials for > 50 MHz developed. New magnetic materials demonstrate magnetic properties equal to or better than those of 30-50 µm nanogranular films. **Completed 12/20/2013** Zinc ferrite nanocrystals from 10 nm to 18 nm in size were produced at multiple gram scale. specifically, 18 nm zinc ferrite nanocrystal keeps quality factor to be higher than 20 up to 74 MHz and higher than 10 up to 150 MHz. 10.5 nm zinc ferrite nanoparticles were integrated into a 25 turn hand wound inductor and achieved 91.9% efficiency in a continuous fan test. Fabrication of third-generation air-core magnetics (for full integration) completed. **Completed 11/30/2012** 3rd generation air-core inductors were fabricated. The inductors consist of 70 turns, with an outer diameter of 8 mm and inner diameter of 4 mm. The inductors are approximately 1 mm in height. The gap between windings showed 100 µm and the winding thickness was 30 µm. Characteristics of third-generation air-core magnetics (inductance, loss, voltage breakdown) successfully validated. **Completed 12/31/2014** As stated earlier, electrical breakdown was never observed to be an issue. By this point the models of inductor inductance and resistance (loss) had been verified against a greatly expanded library of FEA simulations and larger set of experimental data. Most of the experimental data consisted of (low-power) impedance measurements that did not provide thermal stress. The models matched both the simulations and the impedance measurements very well. The modeled inductance was always within a few percent of the measured inductance. At the worst-case frequency, the modeled resistance (loss) was well within 10% of the measured resistance. This should correspond to modeled total power converter efficiency within several percent of the measured efficiency.

Major Tasks	Key Milestones and Deliverables
	Characterization results of the 70-turn inductors showed an inductance of 653 nH, an AC resistance of 2.9 Ohms, and a quality factor of 13.2 at 10 MHz. It has been concluded that coreless ("air-core") inductors needed to meet the program specifications are not sufficiently small to be interesting (as compared to other possibilities), and represent a substantial fabrication / yield risk in practice owing to the high number of needed turns. Attention thus turned from coreless toroidal designs to testing of toroids filled with a magnetic core (e.g., including Dartmouth and Penn material versions and versions with commercial material created at GIT).
Program Element 3: Circuit development and fabrication **3.1**: Topology and control investigation **3.2**: Circuit validation: discrete commercial components **3.3**: Design optimization **3.4**: IC development **3.5**: Circuit validation: discrete custom components **3.6**: Prototype system development: hybrid integration of controls, devices, passives **3.7**: Single chip integration and validation	**Q3**: Completed study of topology and control options. Study will provide a set of at least three suitable topology options and an assessment of their viability as a function of the achievable characteristics of magnetics (e.g., size, inductance, loss, and type [incl. resonant/bulk, cored/coreless, inductor/transformer]) and devices (e.g., breakdown voltages, resistances and capacitances.) **Completed 6/30/2011** A variety of topology options and design tradeoffs were considered. A merged-two-stage circuit architecture was identified to enable operation across large, wide-input voltage ranges while preserving high-frequency capability. For the target application the use of an inverted resonant-transition buck topology was identified as being highly suited to the system requirements. **Q4:** Circuit validation with commercial transistors and magnetics completed. Conversion function demonstrated at input voltage > 100 V and switching frequency > 5 MHz. **Completed 8/31/2011** An inverted resonant-transition buck converter suitable for providing a 35 V output from input voltages exceeding 100 V has been demonstrated with operation at a variable frequency of 5-10 MHz at a few tens of Watts. **Q5**: Initial optimization results: baseline design with recommended devices and magnetic component sizing. Optimization (across circuit design and control) will seek the highest system efficiency achievable within a size envelope determined by the passive components. **Completed 12/15/2011** A simulation and loss-computation tool was developed to enable rapid exploration of the design space. Initial component size optimization for a 50-100V input, 35 V output power stage was

Major Tasks	Key Milestones and Deliverables
	developed. **Q8**: Discrete circuit validation with custom program devices and magnetic components completed. Successful in-circuit operation of individual components at performance levels (voltages, currents, frequencies) required for final system. **Completed 9/14/2012** 1) The 653 nH GIT air core inductor was tested in the circuit with a commercial GaN FET. The efficiency was 82.73% delivering 23.2 watts at a frequency of 8.28 MHz. 2) The first MIT GaN FET was tested in the circuit with commercial inductors. The efficiency was 89.38% delivering 22.8 watts at a frequency of 8.70 MHz. Completed control IC (tapeout). **Completed 8/27/2012** Control integrated circuit tapeout was completed. **Q12**: Completed validation of hybrid integrated system with custom control IC, devices, passives. Demonstration at the following performance level: >100 V input at 10-50 W, >5 MHz switching frequency, >85% efficiency, > 100 W/in^3 component power density. **Completed 9/01/2013** The circuit was tested with the first generation MIT GaN FET and the Dartmouth G2 racetrack inductor. The custom control IC was not used. From 26 watts to 33 watts the efficiency was above 85% and the frequency was above 5 MHz. The peak efficiency was 85.56% delivering 32.67 watts with a frequency of 5.092 MHz. The volume of the power part of the circuit was 0.0555 in^3 for a power density of 588 watts/in^3. **Q14**: Completed co-optimization of circuit topology, devices, magnetics. Optimization (across device sizing/layout, magnetic component design, and circuit design) will seek highest system efficiency achievable within a predetermined size envelope dictated by the passive components. **Completed 12/10/2013** Using the parts that would provide the most efficient circuit with the highest power density, a printed circuit board was designed for the converter. Final integrated power converter validation. Device fabricated and tested with following performance: > 100 V input, 10-50 W, > 93% efficiency, >5 MHz switching frequency, 100 ^{o}C operation, > 300 W/in^3.

Major Tasks	Key Milestones and Deliverables
	Completed 1/22/2014 1) The final circuit was tested with a 100 V input at an output power of 41 watts. The efficiency was 94% and the box power density was 406 W/in^3. The circuit was not tested at 100° C. Though not a program requirement, the circuit develops its own control power and the efficiency includes that power loss. 2) A second circuit which is an AC to DC circuit was also designed and tested. The efficiency was 93.3% with a power factor of 0.89. The box power density was 45 W/in^3. The displacement power density was 130 W/in^3. The switching frequency varied between 3 and 30 MHz depending on where in the AC voltage cycle it was operating.
Program Element 4: Manufacturing & Commercialization Analysis 4.1 Manufacturing analysis 4.2 Technology transfer & outreach (TT&O) and commercialization planning	**Q10:** Analysis and planning of TT&O, as well as commercialization of technologies under development presented and discussed with ARPA-E **Completed 12/04/2012** Discussed commercialization plan with ARPA-E Program Manager. **Q12:** Test follow-on lots of semiconductor devices and magnetic components. Revise estimates of system performance. **Completed 1/14/2014** To evaluate different core materials, hand wound inductors were fabricated on toroidal cores and tested in the circuit with commercial GaN FETs. Most tests were done under pulsed conditions except for UPenn core materials which were found to perform better at higher temperatures. Powdered iron cores suitable for inclusion in microfabricated windings yielded an efficiency of 94.34% at a power of 27.97 watts. Dartmouth fabricated core material yielded a slightly higher efficiency of 94.43% at a power of 42.81 watts. Final samples of the UPenn developed core material yielded a maximum efficiency of 93.19% at 42.65 watts. Third generation MIT GaN FETs were tested in the circuit using commercial inductors. With no cooling they yielded an efficiency of 92.56% at 14.85 watts. With cooling the efficiency improved to 95.51% at 36.29 watts. Begin evaluation of manufacturability of system and estimation of cost. **Completed 12/13/2013** Two demonstration circuits were designed and built at the end of the project. The first contained only the parts necessary to realize a working version of the circuit to meet the specifications for the

Major Tasks	Key Milestones and Deliverables
	project (input voltage = 100 V, output voltage = 35 V, 10-50 watts, >93% efficient, >5 MHz switching). The second also included a microprocessor based control, power supply for the control circuit, startup circuit, and input EMI filter. In approximately 10K quantity, the first circuit should cost $8.40 to manufacture including labor. The second should cost $18.16. Analysis and planning of TT&O, as well as commercialization of technologies under development presented and discussed with ARPA-E. **Completed 9/27/2013** Industry Advisory Committee Meeting was held on Wednesday, May 29th. Twelve representatives from nine companies (Foxconn, Lutron, M/A Com, Maxim, Osram Sylvania, Picor, Samsung, Texas Instruments, and Volterra) participated in the meeting to discuss commercialization opportunities for the results of this research. **Q14:** Final evaluation of system performance relative to industry best-in-class. **Completed 3/13/2014** The DC/DC converter built for this project has better efficiency (94% vs. 83%), better power density (406 W/in^3 vs. <5 W/in^3), and higher frequency operation (5 MHz vs. 104 kHz). More significant may be a comparison of the AC/DC converter, also built using technology from this program, which more closely matches the function of the industry best-in-class devices. The efficiency for the AC/DC converter is higher (93.3% vs. 83%), the power density is higher (45 W/in^3 vs. <5 W/in^3), the frequency is higher (minimum 3MHz vs. 104 kHz) and the power factor is comparable (0.89 vs. 0.93). Also, no one commercial device embodied all these performance characteristics. Each parameter indicated is the best of any of the devices tested. Full assessment of manufacturability, identification of manufacturing gaps, and estimate of in-volume production costs. **Completed 3/13/2014** In section 4.08 initial estimates of the cost of the circuit were made. The bare circuit was $8.40 and the complete circuit was $18.16. Of this cost, the basic power components represented $3.62. The remainder was for the control function which was implemented with off-the-shelf components. We estimate that a custom chip to perform these functions would cost $1.00. The circuit should therefore cost $4.62 or $4.74 if we include the EMI filter.

Major Tasks	Key Milestones and Deliverables
	Analysis and planning of TT&O, as well as commercialization of technologies under development presented and discussed with ARPA-E. **Completed 1/29/2014** Presented poster at Solid State Lighting Conference in Orlando, FL.

Project Activities

To realize advances in power conversion technology, the research project investigated each of new power semiconductor devices, new magnetic materials and component designs, and new circuit architectures and topologies to realize higher degrees of miniaturization, integration and performance of power electronics. The applications focus was on power converters for driving LED loads, encompassing ac-to-dc and dc-to-dc conversion from moderate voltage levels (to above 100 V) to low voltages (e.g., tens of Volts) at low to moderate operating power levels (e.g., tens of Watts). Semiconductor device research focused on the performance, reliability and improved design of devices based on Gallium Nitride (GaN). Magnetics research focused on both development of new magnetic materials suitable to higher operating frequencies and on microfabrication of magnetic components. Systems research focused on leveraging these advances to attain higher operating frequencies, miniaturization and performance as compared to the present state of the art.

Project Outputs

A. Journal Articles

1. “Studies of Liquid Crystalline Self-Assembly of GdF3 Nanoplates by In-Plane, Out-of-Plane SAXS" T. Paik, D. K. Ko, T Gordon, V. Doan-Nguyen, C. B. Murray ACS Nano In Press 2011.
2. "Thiocyanate-Capped Nanocrystal Colloids: Vibrational Reporter of Surface Chemistry and Solution-Based Route to Enhanced Coupling in Nanocrystal Solids" A. T. Fafarman, W-K Koh, B. T. Diroll, D.K. Kim, D-K Ko, S. J. Oh, X. Ye, V. Doan-Nguyen, M. R. Crump, D. C. Reifsnyder, C. B. Murray, and C. R. Kagan, J. Am. Chem. Soc., Article ASAP (Web): August 17, 2011.
3. "Enhanced Thermal Stability and Magnetic Properties in NaCl-Type FePt-MnO Binary Nanocrystal Superlattices" A. Dong, J. Chen, X. Ye, J. M. Kikkawa, and C.B. Murray, J. Am. Chem. Soc., 2011, 133 (34), 13296-13299 2011.

4. “Tri-Gate Normally-off GaN Power MISFET,” B. Lu, E. Matioli and T. Palacios, IEEE Electron Device Letters, vol. 33, no. 3, pp. 360-362, 2012.
5. “A Technology Overview of the PowerChip Development Program” Mark G. Allen, Mohammad Araghchini, Jun Chen, Jesus A. del Alamo, Vicky Doan-Nguyen, Gary DesGroseilliers, Daniel V. Harburg, Florian Herrault, Donghyun Jin, Jungkwun Kim, Min Soo Kim, Jeffrey H. Lang, Christopher G. Levey, Seungbum Lim, Bin Lu, Christopher Murray, David Otten, Tomas Palacios, David J. Perreault, Daniel Piedra, Jizheng Qiu, John Ranson, Charles R. Sullivan, Min Sun, Xuehong Yu, and Hongseok Yun, IEEE Transactions on Power Electronics, Accepted subject to mandatory revisions. Revised version submitted Sept. 10, 2012.
6. "Impact of high-power stress on dynamic ON-resistance of high-voltage GaN HEMTs," D. Jin, J. del Alamo, Microelectron Reliab., to be published, 2012.
7. J. Qiu and C. R. Sullivan, "High-Frequency Resistivity Measurement Method for Multi-Layer Soft Magnetic Films", IEEE Transactions on Power Electronics (accepted).
8. C.R. Sullivan, D. V. Harburg, Jizheng Qiu C.G. Levey and Di Yao, “Integrating Magnetics for on-Chip Power: A Perspective,” IEEE Transactions on Power Electronics, accepted subject to mandatory revisions. Revision submitted Sept. 24, 2012.
9. “MICROFABRICATION OF AIR CORE POWER INDUCTORS WITH METAL-ENCAPSULATED POLYMER VIAS” Jungkwun ‘JK’ Kim, Florian Herrault, Shannon Yu, Mark G. Allen, J. Micromech. Microeng. Aug 2012 (In press)
10. “Silicon-embedding approach to 3-D toroidal inductor fabrication” X.Yu, M.Kim,F.Herrault, C-H. Ji, J.Kim, M.G.Allen , Journal of MEMS, July 2012 (In press)
11. "An Etch-Stop Barrier Structure for GaN High-Electron-Mobility Transistors," B. Lu, M. Sun and T. Palacios, IEEE Electron Device Lett., vol. 34, no. 3, pp. 369-371, Mar. 2013.
12. M. Araghchini, X. Yu, M. S. Kim, F. Herrault, M. G. Allen and J. H. Lang; “Modeling and measured verification of loss in MEMS toroidal inductors”; IEEE Transactions on Industry Applications. Invited and accepted.
13. D. Jin and J. A. del Alamo, "Methodology for the study of dynamic ON-resistance in high-voltage GaN field-effect transistors." IEEE Transactions on Electron Devices, Vol. 60, No. 10, pp. 3190-3196, October 2013.
14. D. Jin and J. A. del Alamo, "Impact of high-power stress on dynamic ON resistance of high-voltage GaN HEMTs." Microelectronics Reliability, Vol. 52, pp. 2875-2879, 2012.
15. S. Lim, J. Ranson, D.M. Otten and D.J. Perreault, "Two-Stage Power Conversion Architecture Suitable for Wide Range Input Voltage," IEEE Transactions on Power Electronics, (Electronic Early Access 2014).

B. Papers

1. Yu, Xuehong; Kim, Minsoo; Herrault, Florian; Ji, Chang-Hyeon; Kim, Jungkwun; Allen, Mark, “ Silicon-embedded 3D toroidal air-core inductor with through-wafer interconnect for on-chip integration ,” MEMS 2011. IEEE 25th International Conference, Paris, France, Jan. 2012.
2. Jin, D and del Alamo, J.A., "Mechanisms responsible for dynamic ON-resistance in GaN high-voltage HEMTs" To be presented at IEEE International Symposium on Power Semiconductor Devices and ICs, Bruges, Belgium, June 3-7, 2012.

3. B. Lu, T. Palacios, D. Risbud, S. Bahl and D. I. Anderson, “Extraction of dynamic on-resistance in GaN transistors under soft- and hard-switching conditions,” IEEE Compound Semiconductor Integrated Circuit Symp. (CSICS), Oct. 2011, pp. 1-4.
4. Jizheng Qiu and Charles R. Sullivan, "Radial-Anisotropy Nanogranular Thin-Film Magnetic Material for Toroidal Inductors,"IEEE Applied Power Electronics Conference and Exposition (APEC), Orlando, FL, Feb. 2012.

5. Jizheng Qiu and Charles R. Sullivan, "Radial-Anisotropy Thin-Film Magnetic Material for High-Power-Density Toroidal Inductors," 7th International Conference on Integrated Power Electronics Systems (CIPS), Nuremberg, Germany, Mar. 2012.
6. Daniel V. Harburg, Xuehong Yu, Florian Herrault, Christopher Levey, Mark Allen, and Charles R. Sullivan. “Micro-fabricated thin-film inductors for on-chip power conversion,” 7th International Conference on Integrated Power Electronics Systems (CIPS), 333-338, Nuremberg, Germany, Mar. 2012.
7. B. Lu, E. Matioli and T. Palacios, “Low-Leakage Normally-Off Tri-Gate GaN MISFET,” 24th IEEE International Symposium on Power Semiconductor Devices and ICs (ISPSD), Bruges, Belgium, Jun. 2012.
8. Jin, D and del Alamo, J.A., "Impact of high-power stress on dynamic ON-resistance of high-voltage GaN HEMTs," IEEE Reliability of Compound Semiconductors (ROCS), Boston, Apr. 2012.
9. Harburg, Daniel V, Qiu, Jizheng and Sullivan, Charles R. "An Improved AC Loss Model for the Optimization of Planar-Coil Inductors," 13th IEEE Workshop on Control and Modeling for Power Electronics (COMPEL), Kyoto, Jun. 2012.
10. M. Araghchini, M. S. Kim, X. Yu, F. Herrault, M. G. Allen and J. H. Lang, "Modeling and Measured Verification of Loss in MEMS Toroidal Inductors", IEEE Energy Conversion Congress and Exposition, Raleigh, NC, September 2012.
11. X.Yu, M.Araghchini, F.Herrault, J.Kim, J.H.Lang, and M.G.Allen, "Fabrication, Modeling and Performance Analysis of Silicon-embedded 3-D Toroidal Inductors," 12th Intl. Workshop on Micro and Nanotechnology for Power Generation and Energy Conversion Applications(PowerMEMS), Atlanta, GA, Dec. 2012.
12. J. Kim, F. Herrault, X. Yu, M. Kim, and M.G. Allen, "Microfabrication of air core toroidal inductor with very high aspect ratio metal-encapsulated polymer vias," 12th Intl. Workshop on Micro and Nanotechnology for Power Generation and Energy Conversion Applications(PowerMEMS), Atlanta, GA, Dec. 2012.
13. J. Qiu, H. Syed, and C. R. Sullivan, "Complex Permeability Measurements of Radial-Anisotropy Thin-Film Magnetic Toroidal Cores", in Joint MMM/Intermag Conference, Jan. 18, 2013. Chicago, Illinois.
14. J. Qiu, D. V. Harburg, and C. R. Sullivan, "A Toroidal Power Inductor Using Radial-Anisotropy Thin-Film Magnetic Material Based on a Hybrid Fabrication Process", in IEEE Applied Power Electronics Conference and Exposition (APEC), March 17-21, 2013 . Long Beach, CA.
15. H. Syed and C.R. Sullivan, “Large-Signal, High Frequency Magnetic Characterization of Toroidal Inductor Cores," in IEEE Applied Power Electronics Conference and Exposition (APEC), March 17-21, 2013. Long Beach, CA.
16. C.R. Sullivan, Jizheng Qiu, D.V. Harburg and C.G. Levey, “Nanogranular magnetic materials for enhanced low-profile inductors,” Invited presentation, IEEE Global Interposer Technology Workshop, November 14-16, 2012. Atlanta, GA.
17. Jungkwun ‘JK’ Kim, Seung-Joon Paik, Florian Herrault, Mark G. Allen, “UV-LED LITHOGRAPHY FOR 3-D HIGH ASPECT RATIO MICROSTRUCTURE PATTERNING,” Hilton Head Workshop 2012:A Solid-

State Sensors, Actuators and Microsystems Workshop, Hilton Head Island, SC. , June 3 - 7, 2012, pp. 481 - 484.

18. Seungbum Lim, John Ranson, David M. Otten, and David J. Perreault, "Two-Stage Power Conversion Architecture for an LED Driver Circuit," in IEEE Applied Power Electronics Conference and Exposition (APEC), March 17-21, 2013. Long Beach, CA.
19. Jizheng Qiu, H. Syed, and C. R. Sullivan, "Complex Permeability Measurements of Radial-Anisotropy Thin-Film Magnetic Toroidal Cores," IEEE Energy Conversion Conference and Exposition (ECCE), Denver, CO, 16 Sept. 2013.
20. D.V. Harburg, Jizheng Qiu, Rui Tian, G.R. Khan, D. Otten, C.G. Levey and C.R. Sullivan "Measured Performance and Micro-Fabrication of Racetrack Power Inductors," IEEE Energy Conversion Conference and Exposition (ECCE), Denver, CO, 16 Sept. 2013 (accepted).
21. Jizheng Qiu and C.R. Sullivan, "Design of Toroidal Inductors with Multiple Parallel Foil Windings," 14th IEEE Workshop on Control and Modeling for Power Electronics (COMPEL), Salt Lake City, 24 June 2013.
22. D. V. Harburg, G. R. Khan, F. Herrault, Jungkwun Kim, Christopher G. Levey, and C. R. Sullivan, "On-Chip RF Power Inductors With Nanogranular Magnetic Cores Using Prism-Assisted UV-LED Lithography," 17th International Conference on Solid-State Sensors, Actuators and Microsystems, Barcelona, Spain, 17 June 2013.
23. M. Araghchini and J. H. Lang; "Modeling, design, fabrication and testing of MEMS toroidal inductors for integrated power electronic applications", Proceedings of the MIT MTL Microsystems Annual Research Conference (MARC), Cambridge, MA, January 2013.
24. M. Araghchini and J. H. Lang; "Modeling and analysis of Silicon-embedded 3-D Toroidal Inductors"; Proceedings of the PowerMEMS Conference, London, UK, December 3, 2013. Accepted.
25. M. Araghchini, X. Yu, F. Herrault, J. Qiu, C. R. Sullivan, M. G. Allen and J. H. Lang; "Modeling and measured verification of loss in MEMS toroidal inductors"; 3rd International Workshop on Power Supply on Chip (PowerSoC2012), San Francisco, CA, Nov 16, 2012.
26. D. Jin, J. Joh, S. Krishnan, N.Tipirneni, S. Pendharkar and J. A. del Alamo, "Total current collapse in high-voltage GaN MIS-HEMTs induced by Zener trapping." IEEE International Electron Devices Meeting, Washington DC, December 9-11, 2013.
27. S. Lim, D.M. Otten and D.J. Perreault, "Power Conversion Architecture for Grid Interface at High Switching Frequency," 2014 IEEE Applied Power Electronics Conference, March 2014.
28. M. Araghchini, J. Lang, "Modeling, Design and Performance of Integrated Power Electronics using MEMS Toroidal Inductors", proceedings of IEEE Conference Applied Power Electronics Conference and Exposition (APEC) 2014, pages 519-526.
29. M. Araghchini, J. Lang, "Modeling, Fabrication and Characterization of Integrated Toroidal Inductors for Power Electronics Applications", proceedings of MTL Annual Research Conference (MARC), Bretton Woods, NH, January 2014, 2.03, page 31.

C. Status Reports

1. Status Report 1.1: Devices, February 4, 2011
2. Status Report 2.1: Magnetics, February 4, 2011
3. Status Report 3.1: Circuits and Systems, February 4, 2011
4. Status Report 1.2: Devices, March 31, 2011
5. Status Report 2.2: Magnetics, March 31, 2011

6. Status Report 3.2: Circuits and Systems, March 31, 2011
7. Status Report 1.3: Devices, June 30, 2011
8. Status Report 2.3: Magnetics, June 30, 2011
9. Status Report 3.3: Circuits and Systems, June 30, 2011
10. Status Report 1.4: Devices, September 28, 2011
11. Status Report 2.4: Magnetics, September 28, 2011
12. Status Report 3.4: Circuits and Systems, September 28, 2011
13. Status Report 1.5: Devices, December 28, 2011
14. Status Report 2.5: Magnetics, December 28, 2011
15. Status Report 3.5: Circuits and Systems, December 28, 2011
16. Status Report 1.6: Devices, March 30, 2012
17. Status Report 2.6: Magnetics, March 30, 2012
18. Status Report 3.6: Circuits and Systems, March 30, 2012
19. Status Report 1.7: Devices, June 28, 2012
20. Status Report 2.7: Magnetics, June 28, 2012
21. Status Report 3.7: Circuits and Systems, June 28, 2012
22. Status Report 1.8: Devices, September 30, 2012
23. Status Report 2.8: Magnetics, September 30, 2012
24. Status Report 3.8: Circuits and Systems, September 30, 2012
25. Status Report 1.9: Devices, December 31, 2012
26. Status Report 2.9: Magnetics, December 31, 2012
27. Status Report 3.9: Circuits and Systems, December 31, 2012
28. Status Report 1.10: Devices, March 31, 2013
29. Status Report 2.10: Magnetics, March 31, 2013
30. Status Report 3.10: Circuits and Systems, March 31, 2013
31. Status Report 1.11: Devices, June 28, 2013
32. Status Report 2.11: Magnetics, June 28, 2013
33. Status Report 3.11: Circuits and Systems, June 28, 2013
34. Status Report 1.12: Devices, September 28, 2013
35. Status Report 2.12: Magnetics, September 28, 2013
36. Status Report 3.12: Circuits and Systems, September 28, 2013

D. Media Reports

1. Dartmouth Engineer, Summer 2010. http://www.dartmouthengineer.com/2010/09/kudos-summer-2010/
2. Dartmouth Engineering Professors Awarded Clean Energy Technologies Grants from DoE, Thayer School of Engineering at Dartmouth, Press Release, July 22, 2010. http://engineering.dartmouth.edu/news-events/press/ARPA-E.html
3. Penn Nanoparticle Assembly Effort Attracts Science Magazine Editor's Choice.

http://www.sciencemag.org/content/332/6026/twil.full

E. Invention Disclosures

1. Bin Lu, Elison Matioli and Tomás Palacios, "Advanced substrates for GaN power electronics," December 2010.
2. David J. Perreault, John D. Ranson and Seungbum Lim, "HF Switched LED Driver with Switched-Capacitor Pre-regulator," April 2011.
3. Bin Lu, Elison Matioli and Tomás Palacios, “New structure and technology for power semiconductor devices”, Oct. 11, 2011.
4. David Perreault, Seungbum Lim and David Otten, "Grid Interfaced Power Conversion Architecture," March 2013.

F. Patent Applications

1. Jizheng Qiu and Charles R. Sullivan, "Systems And Methods For Making Radial Anisotropic Thin-Film Magnetic Torroidal Cores, And Cores Having Radial Anisotropy," Provisional patent filed 22-September-2011.
2. Daniel Harburg, Christopher Levey, Jason Stauth, and Charles Sullivan, "Microfabricated Magnetic Devices and Associated Methods," U.S. provisional patent No. 61/657,186 filed June 8th, 2012.
3. D.J. Perreault, S. Lim and D.M. Otten, “Grid Interface Power Conversion Architecture,” Provisional Patent, Filed April 9, 2013.

G. Licensed Technologies

No technologies licensed.

H. Networks/Collaborations Fostered

1. Industry Advisory Committee Meeting was held on Wednesday, May 29th. Twelve representatives from nine companies (Foxconn, Lutron, M/A Com, Maxim, Osram Sylvania, Picor, Samsung, Texas Instruments, and Volterra) participated in the meeting to discuss commercialization opportunities for the results of this research.

I. Websites Featuring Project Work Results

No websites featuring project work or results.

J. Other Products (e.g. Databases, Physical Collections, Audio/Video, Software, Models, Educational Aids or Curricula, Equipment or Instruments)

No other products.

K. Awards, Prizes, and Recognition

1. Penn Materials Chemist was awarded an Honorary Doctorate from the University of Utrecht in the Netherlands for discovery and development of quantum dot (semiconductor nanocrystal) based material for Sutainable Energy". http://www.dub.uu.nl/content/eredoctor-chris-murray-nieuwe-materialen
2. Tomas Palacios (MIT) was awarded the Presidential Early Career Award for Scientists and Engineers (PECASE) for his contributions to GaN and graphene electronics.
3. Donghyun Jin (MIT) was awarded the ISPSD '12 Charitat Award-Runner-up at the 24th IEEE International Symposium on Power Semiconductor Devices and ICs (ISPSD).

4. David Perreault (MIT) was elected as IEEE Fellow for "contributions to design and application of very high frequency power electronic converters."
5. Bin Lu, Elison Matioli and Tomas Palacios (MIT) are awarded the 2012 IEEE Electron Devices Society George Smith Award for the paper "Tri-Gate Normally-Off GaN Power MISFET" published in the 2012 March issue of IEEE Electron Device Letters (EDL).
6. "A Technology Overview of the PowerChip Development Program" overview paper made the list of IEEE's top downloads for the month of May: #45 most popular in all of the IEEE publications, and the #1 download for the Transactions on Power Electronics.
7. Charles R. Sullivan was elevated to IEEE Fellow in January 2014 for "… contributions to the design of power electronic circuits and magnetics."

Follow-On Funding

Additional funding committed or received from other sources (e.g. private investors, government agencies, nonprofits) after effective date of ARPA-E Award.

Table 2. Follow-On Funding Received.

Source	Funds Committed or Received
Texas Instruments	$180k to Dartmouth for "Batch Fabrication of Radial Anisotropy Toroidal-Core Magnetics for Power Applications."
Texas Instruments	$80k to MIT for "High-Frequency High-Density Power Converter."